Retraction for *Nanoscale*:

Design of nanoporous metals with bimodal pore size distributions for enhanced biosensing

Huajun Qiu, Xiaochen Dong and Xirong Huang

Nanoscale, 2012, 4492–4497 (DOI: 10.1039/C2NR30460K). **Retraction published 26 September 2012**

We, the named authors, hereby wholly retract this *Nanoscale* article, due to unreliable experimental results which cannot be repeated.

Signed: Huajun Qiu, Xiaochen Dong and Xirong Huang, China, September 2012

Retraction endorsed by Philip Earis, Managing Editor.

Nanoscale

Dynamic Article Links

Cite this: *Nanoscale*, 2012, **4**, 4492

www.rsc.org/nanoscale

PAPER

Design of nanoporous metals with bimodal pore size distributions for enhanced biosensing†

Huajun Qiu,*[ac] Xiaochen Dong[b] and Xirong Huang[a]

Received 26th February 2012, Accepted 27th March 2012
DOI: 10.1039/c2nr30460k

Nanoporous gold (np-Au) has shown great potential in catalysis, plasmonics, sensing, *etc.* In this work, by two-step dealloying a well-designed AuAgAl ternary precursor alloy, np-Au with bimodal ligament/pore size distributions is successfully fabricated. The first dealloying in HCl solution removes Al and generates a nanoporous AuAg alloy which would be mildly annealed at 200 °C for 30 min to homogenize the alloy ligament and enlarge the ligament/pore size. Next, the nanoporous AuAg alloy is further dealloyed in a HNO_3 solution to etch Ag and fabricate np-Au with a hierarchical microstructure. This novel bimodal np-Au is demonstrated to exhibit enhanced electrocatalytic activity towards H_2O_2 reduction and be a better support for the fabrication of an oxidase-based biosensor compared with normal np-Au, with a uniform pore/ligament size of 30–40 nm. In a proof-of-concept study, a sensitive glucose biosensor with a linear range up to 21 mM is fabricated by immobilization of glucose oxidase on the bimodal np-Au.

1. Introduction

Nanoporous metals have recently attracted considerable interest in a wide variety of applications including catalysis, fuel cells, sensors, actuators, microfluidic flow controllers, and so forth.[1–21] Template methods are commonly used to fabricate these materials through the replication of porous alumina or liquid-crystal templates.[22–24] These methods have the advantages of precise control over the pore size and microstructure periodicity but normally result in materials with one-dimensional porosity, such as an array of tubes.[23] Recently, dealloying, which refers to the selective dissolution of one or more components out of an alloy, has received significant attention for the fabrication of nanoporous metals with an open, bicontinuous ligament–pore structure.[25] Although various nanoporous metals have been prepared by the dealloying route, nanoporous gold (np-Au) prepared by dealloying AuAg alloy is of special interest due to not only its unique mechanical and physicochemical properties but also its biocompatibility.[2,25–31] For example, due to its tunable pore size, excellent electron conductivity and biocompatibility, np-Au has been demonstrated to be a good support for enzymes and the fabrication of electrochemical biosensors.[31]

Fabrication of nanostructured materials with controllable morphology and size is very important for studying the structure/size-related properties and their potential applications. For np-Au obtained by dealloying, it has been demonstrated that its microstructure (pore/ligament size) can be tailored by changing the alloy compositions, dealloying conditions, and annealing conditions after dealloying.[25,32] However, np-Au prepared by simply changing these experimental parameters is homogeneous in microstructure. For specific applications, the fabrication of nanoporous metals with hierarchical microstructure is more desirable. For example, in microfluidic-based sensors, larger sized pores (hundreds of nm) are useful in microfluidic flow control, whereas small pores (tens of nm) are useful for increasing device surface area and sensitivity. For some enzyme-based biosensors, the large pores facilitate the loading of enzymes and the small pores/ligaments with high surface area facilitate the mass transfer of small molecules of substrates/products and give a sensitive response. However, the fabrication of np-Au with hierarchical structure by the dealloying strategy has been rarely reported. Ding and Erlebacher[33] reported a dealloying/Ag plating/redealloying strategy to create np-Au with bimodal pore size distributions. In their work, np-Au is used as the template for Ag plating, and then annealing is applied to homogenize the Ag with Au and enlarge the pore size. The second dealloying would then result in the second modal pore. Zhang and co-workers[16] reported the fabrication of bimodal np-Au by dealloying AuAl alloy which contains both pure Al phase and $AuAl_2$ phase. Large channels of several micrometres are formed by the dissolution of pure Al phase and the nanopores are formed by dealloying the $AuAl_2$ phase.

[a]*School of Chemistry and Chemical Engineering, Shandong University, Jinan 250100, China. E-mail: qiuhuajun@gmail.com*
[b]*Key Laboratory for Organic Electronics & Information Displays, Institute of Advanced Materials, Nanjing University of Posts and Telecommunications, 9 Wenyuan Road, Nanjing, 210046, China*
[c]*WPI Advanced Institute for Materials Research, Tohoku University, Sendai 980-8577, Japan*
† Electronic supplementary information (ESI) available. See DOI: 10.1039/c2nr30460k

In this work, we report on the design and fabrication of bimodal np-Au with high a void space (~92.5%, estimated by the atomic ratio of the precursor alloy) and low density by a simple two-step dealloying process. By sequentially leaching away the active components in a reasonably designed AuAgAl ternary alloy, the resulting material shows a unique bimodal nanoporous structures. Moreover, this bimodal np-Au with high void space is demonstrated to be a better substrate for enzyme-based electrochemical biosensor fabrication compared with normal np-Au with a pore/ligament size of 30–40 nm.

2. Experimental

2.1. Reagents

Glucose oxidase (GOx) was purchased from Sigma-Aldrich. Ascorbic acid (AA), acetamidophenol (AP), uric acid (UA), H_2O_2 and glucose (analytical grade) were purchased from Sinopharm Chemical Reagent Ltd. Co. Other chemicals were also of analytical grade. Triply distilled water and 0.1 M PBS (pH 7.0) were used throughout the experiments.

2.2. Preparation and characterization of nanoporous metals

$Au_{7.5}Ag_{17.5}Al_{75}$ and $Au_{30}Ag_{70}$ (at.%) alloy foils with thickness of ~50 μm were made by melting high purity (>99.9%) Au, Ag, and/or Al in argon atmosphere, followed by cold-rolling on a cold-rolling device (a product from Shanghai Engineering Machinery Factory). For the AuAgAl ternary alloy, the first dealloying was carried out in 1 M HCl solution to remove Al. The dealloyed sample was then washed carefully with pure water and annealed for 30 min at 200 °C. After cooled to room temperature, the annealed sample was immersed into a concentrated HNO_3 solution (~65%) for 1 h to remove Ag. The uniform np-Au with a pore/ligament size of 30–40 nm was obtained by dealloying the $Au_{30}Ag_{70}$ alloy for 1.5 h in a concentrated HNO_3 solution (~65%). $Pt_5Cu_{20}Al_{75}$ ternary alloy was also prepared in a similar way. To fabricate np-Pt, the PtCuAl alloy was first completely dealloyed in 1 M NaOH solution and then annealed for 30 min at 200 °C, followed by dealloying for 30 min in HNO_3 solution (~65%). The microstructure of these samples was characterized with a JEOL JSM-6700F field emission scanning electron microscope (SEM) equipped with an Oxford INCA x-sight Energy Dispersive X-ray Spectrometer (EDS) and a JEM-2100 high-resolution transmission electron microscope (TEM). X-ray diffraction (XRD) analysis was carried out on a Bruker D8 advanced X-ray diffractometer using Cu KR radiation at a step rate of $0.04° \ s^{-1}$.

2.3. Preparation of enzyme/np-Au electrode and biosensing

GOx was immobilized on np-Au (size: 3 mm × 3 mm) by dropping 4 μL GOx stock solution (5 mg mL^{-1}) on the np-Au surface and drying at 4 °C. Then, to avoid leakage of GOx, a 2 μL of Nafion (0.5 wt%) was cast and dried again at 4 °C. The glucose biosensor was made by connecting the one side sealed GOx/np-Au with a gold wire by conducting resin because np-Au is a macroscopic nanomaterial. When not in use, the Nafion/GOx/np-Au was kept in a refrigerator at 4 °C. The current–time curves for glucose biosensing with the enzyme-modified electrodes were recorded at −0.3 V in 10 mL of stirred air-saturated PBS (pH 7.0, 0.1 M). An aliquot of glucose (2.0 M) stock solution was injected into the base solution at regular intervals. Each addition increased the concentration of glucose by 1.5 mM.

All electrochemical experiments were performed on a CHI 660C electrochemical workstation (CH Instrument company) at room temperature. A three-electrode system was used, including a np-Au-based working electrode, a platinum wire counter electrode and a saturated calomel electrode (SCE) reference electrode. All the potentials given in this paper were *vs.* SCE.

3. Results and discussion

3.1. Fabrication of nanoporous metals with bimodal pore/ligament size distributions

It is well-known that selective dissolution of active species from a well-designed alloy results in the formation of a porous structure with nanosized ligaments and pores. Based on the typical example of dealloying AuAg alloy to prepare np-Au, Erlebacher *et al.* (2001) explained the formation mechanism of the nanoporous structure through an atomistic model.[26] This model involves a kind of "interfacial phase separation" in which the active atoms (Ag) are dissolved and the noble atoms (Au) left from the alloy/electrolyte interface would self-organize and form islands and pores/channels. Once the porosity forms, due to the fast surface diffusion of surface noble atoms (Au) in an electrolyte, further dealloying still occurs.

In this work, this dealloying strategy is used to prepare np-Au with bimodal pore size distributions by a two-step dealloying of reasonably designed $Au_{7.5}Ag_{17.5}Al_{75}$ ternary alloy. The first dealloying would produce a nanoporous AuAg alloy with uniform distribution of large-size pores/ligaments and second dealloying would further etch away the second active component (Ag) within the large ligaments, generating the small pores and Au ligaments. For the design of the ternary precursor alloy, considering the rich supply and active property of Al, Al-based alloy was chosen as the precursor alloy. In our previous work, it has been demonstrated that AgAl alloy with a composition of $Ag_{25}Al_{75}$ (at.%) is suitable for the preparation of uniform nanoporous Ag.[34] Thus, in this work, for the AuAgAl ternary alloy, the Al content was set as 75 at.% and the other two noble components were 25 at.% in all. For the AuAg alloy, it is known that $Au_{30}Ag_{70}$ (at.%) is suitable for the dealloying and preparation of np-Au.[25] Therefore, AuAgAl alloy with the nominal composition of $Au_{7.5}Ag_{17.5}Al_{75}$ was chosen as the ternary precursor alloy for the fabrication of np-Au with bimodal pore size distributions. Note that AuAgAl ternary alloys with other alloy ratios deserve further study and are not included in this work.

The composition of the AuAgAl ternary alloy was controlled by the initial feed ratio of pure metals during the refining process and further confirmed by compositional analysis with EDS (Fig. S-1a in ESI†). Fig. 1a shows the SEM image of the sample after the first dealloying in 1 M HCl solution. It is observed that the dealloyed sample exhibits a uniform bicontinuous ligament-pore structure with the ligament/pore size of ~50 nm (estimated by averaging 20 different ligaments/pores in the SEM image). EDS analysis (Fig. S-1b in ESI†) shows that Al has been completely removed by the first dealloying and the contents of

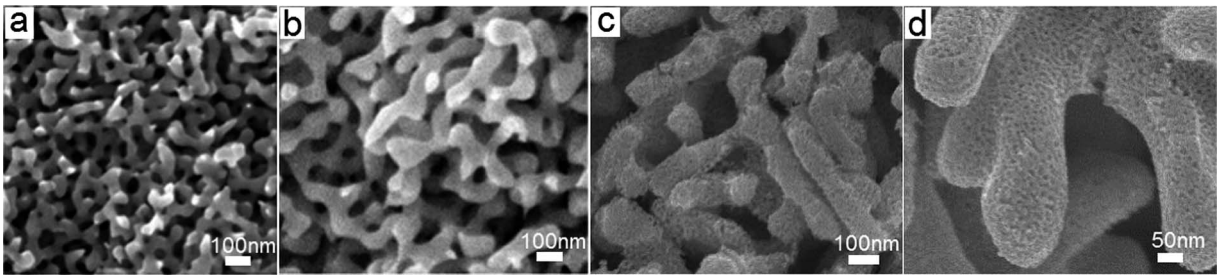

Fig. 1 SEM images of np-AuAg alloy obtained by dealloying the AuAgAl alloy in HCl solution (a), annealed np-AuAg alloy (b), bimodal np-Au obtained by further dealloying the np-AuAg in HNO_3 solution (c), and (d) is the enlarged SEM image of the bimodal np-Au.

Au and Ag change negligibly. Thus, the product obtained after the first dealloying is the nanoporous $Au_{30}Ag_{70}$ alloy. Before the second dealloying in a concentrated HNO_3 solution, the nanoporous AuAg alloy was annealed at 200 °C for 30 min. Annealing would enlarge the ligament/pore size and make the AuAg alloy more uniform. As shown in Fig. 1b, the ligament/pore size increased to ~90 nm after the annealing with the nanoporous structure well-preserved. The second dealloying in HNO_3 solution then generates the small pores within the large AgAu alloy ligaments, forming the bimodal pore size distributions (Fig. 1c). The enlarged SEM image in Fig. 1d clearly shows that the secondary ligament/pore structure with a typical size of ~10 nm is formed within the large ligaments. EDS analysis (Fig. S-1c in ESI†) indicates that after the second dealloying, the Ag content is less than 8 at.%. The residual Ag in np-Au has also been observed elsewhere when dealloying the bulk AuAg alloy.[27] The residual Ag is believed to be trapped inside the Au ligaments and cannot be removed by simply extending the etching times (up to 100 h).[25] The removal of the active components by dealloying is also confirmed by the weight loss of the precursor alloy which is in good agreement with the theoretical value (data not shown). The size of the precursor alloy changes negligibly after the two-step dealloying, however, the color shows a clear change from silver white of the precursor alloy and np-AuAg to deep brown of the bimodal np-Au. It is worth mentioning that the pore sizes of the bimodal np-Au can also be adjusted to some extent by controlling the dealloying and annealing conditions. For example, the big pore size can be tuned within 100s of nm by controlling the annealing temperature/time and the small pore size can be tuned within ~50 nm by changing the dealloying time. Moreover, the bimodal np-Au is monolithic and has good structure stability, which facilities its application in sensors, actuators, *etc.*

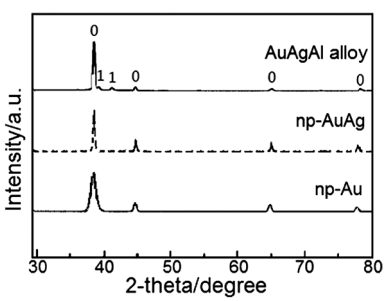

Fig. 2 XRD patterns of the AuAgAl precursor alloy, np-AuAg alloy, and bimodal np-Au.

The changes of crystal structure of the alloy with each dealloying were monitored by XRD (Fig. 2). It is observed that for the ternary precursor alloy, due to the large amount of Al and Ag, the α-AgAl phase (denoted as 0) dominates and a small amount of other alloy phases (Ag_2Al, denoted as 1) can also been detected. However, both SEM and EDS analysis show that the presence of other alloy phases does not affect the complete removal of Al and formation of uniform np-AuAg alloy structure. XRD analysis also shows the face-centered cubic (fcc) AuAg alloy nature of the sample obtained by the first dealloying. It is known that during the dealloying of AuAg alloys, the crystal lattice orientation is retained. This result has also been observed in this work (Fig. 2). It is worth mentioning that due to the formation of ultrafine Au crystal ligaments (~10 nm), the diffraction peaks from the bimodal np-Au are broader than those of the np-AuAg alloy.

It is expected that this fabrication strategy will also be applicable for the preparation of other nanoporous metals by wisely designing the precursor alloys and controlling the dealloying conditions. To demonstrate the versatility of this strategy, np-Pt has also been successfully fabricated by two-step dealloying of the $Pt_5Cu_{20}Al_{75}$ precursor alloy. As shown in Fig. 3a and b, the as-prepared np-Pt also exhibits a well-defined bimodal porous structure with a big pore/ligament size of ~70 to 80 nm and small pore/ligament size of ~3 nm. It is worth mentioning that due to the very low diffusion rate of Pt adatoms (3.6×10^{-22} m^2 s^{-1} which is much smaller than that of Au (2.2×10^{-19} m^2 s^{-1} in vacuum at room temperature))[8] during the second dealloying, the size of the secondary pore is very small (~3 nm), thus, TEM was used to characterize these fine pores. As shown in Fig. 3b, the clear contrast between the dark ligaments and bright pores demonstrates the formation of secondary pores within the big ligaments. XRD analysis (Fig. 3c) further demonstrates the fcc structure of the np-PtCu alloy after the first dealloying in NaOH solution. The (111) diffraction peak of the np-PtCu locates at ~42.54° which is in good agreement with the values calculated by Vegard's law (42.58° for $Pt_{20}Cu_{80}$).[35] After the second dealloying, the three diffraction peaks can be ascribed to fcc pure Pt, indicating the removal of Cu. It is also observed that the diffraction peaks from np-Pt are much wider than those from np-PtCu due to the formation of ultrafine Pt ligaments (~3 nm).

3.2. Bimodal np-Au-based electrochemical biosensor

Np-Au has been demonstrated to be a good substrate for biomacromolecules (such as protein and DNA) and the fabrication

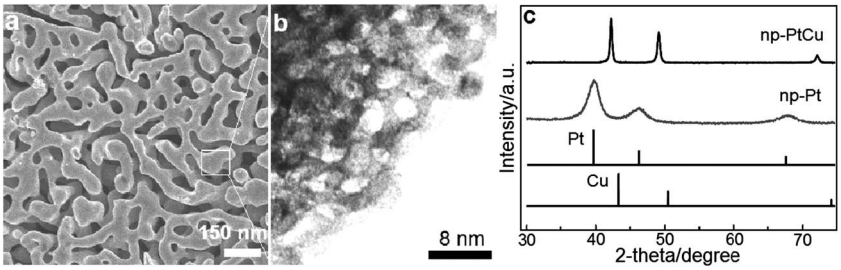

Fig. 3 SEM image of the bimodal np-Pt (a), TEM image of a part of ligament (b) and XRD patterns of np-PtCu and np-Pt (c).

of electrochemical bio-nanodevices due to its large surface area, controllable pore size, good electron conductivity and biocompatibility.[12,36–38] In the present study, this monolithic bimodal np-Au with big pore/ligament size of ~90 nm and small pore/ligament size of ~10 nm is used for an enzyme-based electrochemical biosensor fabrication. The big pores are used as the container for enzyme (GOx is selected as the model), while the small pores/ligaments with a large surface area act as a detector for the enzymatic product with fast response and high sensitivity. It is worth mentioning that due to the comparable size of GOx (~8 nm after hydration)[39] and the small pore (~10 nm), GOx cannot enter most of the small pores.[37]

Before testing the performance of the electrochemical biosensor for glucose, the electrocatalytic activity of the bimodal np-Au towards H_2O_2 (the product of GOx catalyzed oxidation of glucose) reduction was first studied. For comparison, normal np-Au with a uniform pore size of 30–40 nm is also tested. As observed in Fig. 4A, both of the two np-Au electrodes show large H_2O_2 reduction peaks between −0.3 and −0.4 V. In comparison, the bimodal np-Au with an ultrafine pore/ligament size of ~10 nm shows a clearly larger current response for H_2O_2 reduction. Moreover, the peak potential is slightly negatively shifted by ~40 mV, indicating the enhanced electrocatalytic activity of the bimodal np-Au surface. The larger current response should be caused by the larger surface area by forming the small pores. In addition, the Au ligament with a smaller size has a more strained surface and contains more low coordinated surface sites,[40] which should explain the improved electrocatalytic activity of the bimodal np-Au. The enhanced catalytic activity of nanoscaled Au catalyst with a smaller particle size has also been observed elsewhere.[41–43] The high electrocatalytic activity of the np-Au electrodes suggests their potential application in non-enzymatic H_2O_2 sensing. As shown in Fig. 4B, both the electrodes respond rapidly to the addition of H_2O_2 and reach the maximum steady-state current within 4 s, indicating the free diffusion of H_2O_2 into the three-dimensional porous structure and fast electro-reduction. In comparison, the bimodal np-Au electrode exhibits a higher current response, which is in good agreement with that obtained by a linear sweep voltammetry study. The bimodal np-Au also exhibits a wider linear range for H_2O_2 determination (0.05–1.55 mM, $R = 0.997$) compared with uniform np-Au (0.05–1.35 mM, $R = 0.996$; inset in Fig. 4B). This detection limit is ~2 μM ($S/N = 3$) which is even lower than certain horseradish peroxidase (detection limit: 12.89 μM)[44] and carbon nanotube (CNT; detection limit: 10 μM)[45] based biosensors.

The excellent performance of the np-Au electrodes towards H_2O_2 detection suggests that they are promising for the fabrication of oxidase-based biosensors. For the GOx-based biosensor fabrication, first, the amount of GOx loaded was optimized and 20 μg GOx was immobilized on the electrode to ensure a fast conversion of glucose to H_2O_2. The performances of the two np-Au-based glucose biosensors were then tested by recording their amperometric response to the added glucose under −0.3 V (*vs.* SCE). It is worth mentioning that at this low potential the current from the direct oxidation of glucose on np-Au is negligible. Fig. 5a shows the amperometric responses of the two np-Au biosensors towards each addition of 1.5 mM glucose. As observed, this novel bimodal np-Au-based biosensor responses more sensitively to each addition of glucose. The signal

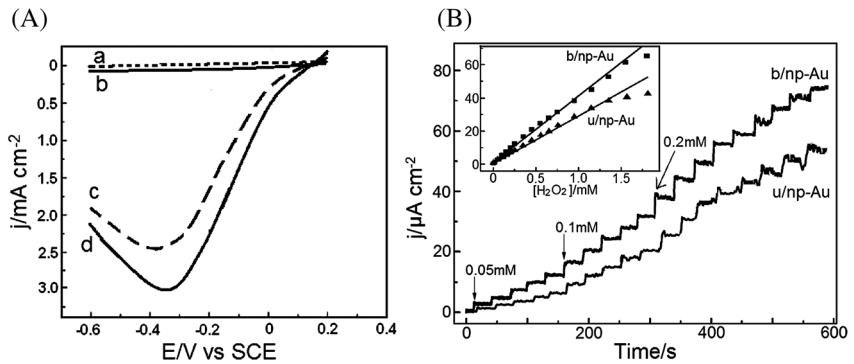

Fig. 4 Linear sweep voltammetry (LSV) curves of uniform np-Au (u/np-Au) with a pore/ligament size of 30–40 nm (a and c), and bimodal np-Au (b/np-Au) (b and d) in PBS (50 mM, pH 7.0) with (c and d) and without (a and b) 5 mM H_2O_2 (A); current responses of the b/np-Au and u/np-Au electrode on successive addition of H_2O_2 at −0.3 V (B), inset in (B) is the corresponding plots of currents *vs.* H_2O_2 concentrations.

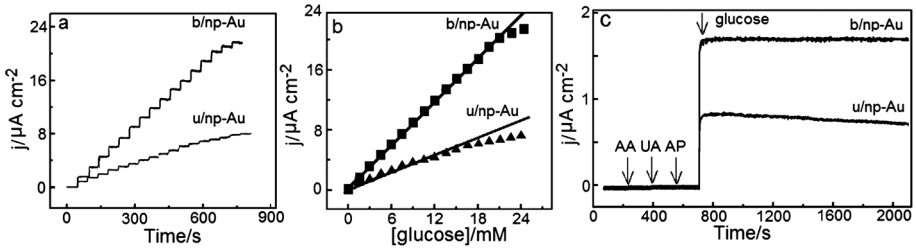

Fig. 5 Current responses of GOx/bimodal np-Au and GOx/uniform np-Au on successive addition of 1.5 mM glucose into a stirring PBS (50 mM, pH 7.0), applied potential: −0.3 V (a); plots of currents *vs.* glucose concentrations (b); current responses of the two GOx modified electrodes on the addition of AA (~0.1 mM), AP (~0.1 mM), UA (~0.02 mM), and glucose (1.5 mM).

reaches the highest value within 4 s, indicating that after the immobilization of GOx on the big pores, glucose can still diffuse freely into the bimodal nanoporous structure and the product from GOx-catalyzed reaction (H_2O_2 here) can be quickly detected. As shown in Fig. 5b, it exhibits a good linear range from 0 to 21 mM ($R = 0.996$) for glucose sensing with a detection limit of ~10 μM ($S/N = 3$). In comparison, the uniform np-Au-based biosensor has a much lower response and shorter linear range (0–18 mM). The linear range of this bimodal np-Au-based biosensor is also wider than other biosensors such as GOx/CNT/Teflon (2–20 mM),[46] GOx/graphene (0.01–10 mM),[47] GOx/nanoporous PtNi (0.5–21 mM),[48] GOx/porous gold (1–18 mM), and GOx/AuPd/graphene (0–3.5 mM)[49] biosensors. The enhanced performance of the bimodal np-Au biosensor can be safely ascribed to its high activity for H_2O_2 electro-reduction. However, it is interesting to observe that after GOx immobilization, the current difference on the two np-Au-based biosensors (Fig. 5a) becomes much larger compared with that on the two bare np-Au sensors (Fig. 4b), *i.e.*, after GOx immobilization, the bimodal np-Au-based sensor is more superior. For example, at 400 s, the current density on GOx/bimodal np-Au is nearly 3 times that on GOx/uniform np-Au, while the current density on bare bimodal np-Au is only ~1.4 times that on uniform np-Au. We assume that with the bimodal pore size distributions, the bimodal np-Au might be easier for the mass transfer of small molecules after GOx immobilization compared with uniform np-Au with pore size of 30–40 nm. In addition, it is believed that after GOx immobilization, the active surface area of np-Au would decrease due to GOx adsorption. For the bimodal np-Au, GOx can only be trapped in the big pores (big ligament surface), thus, the active surface from the small Au ligaments should be better preserved. These factors might explain the superior performance of the bimodal np-Au after GOx loading. As shown in Fig. 5c, the physiological level of AA (0.1 mM), UA (0.02 mM) and AP (0.1 mM) only result in negligible amperometric responses at the two np-Au biosensors due to the low potential applied and the permselective barrier effect of the Nafion membrane. All these suggest that the great potential of the bimodal np-Au-based biosensor for fast, sensitive and selective glucose detection. Moreover, the bimodal np-Au-based biosensor is also reproducible and stable. For 5 mM glucose, the relative standard deviation (RSD) of five freshly prepared np-Au biosensors is ~4.5%. After 1 month storage at 4 °C, the response of the biosensor remains ~97% of its initial value. Note that uniform np-Au also exhibits excellent reproducibility and storage stability. After continuous working for more than 20 min, the current response on the bimodal np-Au-based biosensor changes negligibly, while that on uniform np-Au decreases to ~90% of the initial value (Fig. 5c). These results indicate that the bimodal np-Au is very promising for the fabrication of bio-macromolecule-based (such as enzyme- or DNA-based) biosensors.

4. Conclusions

By two-step dealloying well-designed AuAgAl ternary alloy, np-Au with bimodal pore/ligament size distributions is successfully fabricated. This novel hierarchical np-Au with high void space (92.5%) and low density is demonstrated to be an excellent support for the fabrication of enzyme-based biosensors. The large pores are used as an enzyme container and the small pores/ligaments act as the detector for the enzymatic product to give a signal. In a poof-of-concept study, GOx-loaded bimodal np-Au with pore sizes of ~90 nm and ~10 nm can more sensitively detect glucose up to 21 mM compared with GOx-loaded normal np-Au with a uniform pore size of 30–40 nm. Moreover, this two-step dealloying strategy can also be applied to other systems to prepare other nanoporous metals such as np-Pt. This kind of bimodal nanoporous structure is interesting for both fundamental research and practical applications in sensors, actuators, fuel cells, photocells, *etc.*

Acknowledgements

We acknowledge the support from Shandong University, the Japan Society for the Promotion of Science (JSPS), NNSF of China (20973103, 21173133, 50902071, 61076067), the National Basic Research Program of China (2011CB707400, 2012CB933301), and the Ministry of Education of China (IRT1148).

References

1 Y. Ding, M. W. Chen and J. Erlebacher, *J. Am. Chem. Soc.*, 2004, **126**, 6876.
2 V. Zielasek, B. Jurgens, C. Schulz, J. Biener, M. M. Biener, A. V. Hamza and M. Baumer, *Angew. Chem., Int. Ed.*, 2006, **45**, 8241.
3 Y. Xia, W. Huang, J. F. Zheng, Z. J. Niu and Z. L. Li, *Biosens. Bioelectron.*, 2011, **26**, 3555.
4 A. K. M. Kafi, A. Ahmadalinezhad, J. Wang, D. F. Thomas and A. Chen, *Biosens. Bioelectron.*, 2010, **25**, 2458.
5 Y.-J. Lee and J.-Y. Park, *Biosens. Bioelectron.*, 2010, **26**, 1353.
6 F. Yu, S. Ahl, A.-M. Caminade, J.-P. Majoral, W. Knoll and J. Erlebacher, *Anal. Chem.*, 2006, **78**, 7346.
7 J.-F. Huang and I. W. Sun, *Chem. Mater.*, 2004, **16**, 1829.

8 Z. Zhang, Y. Wang, Z. Qi, W. Zhang, J. Qin and J. Frenzel, *J. Phys. Chem. C*, 2009, **113**, 12629.
9 F. Jia, C. Yu, K. Deng and L. Zhang, *J. Phys. Chem. C*, 2007, **111**, 8424.
10 L. Zhang, X. Lang, A. Hirata and M. Chen, *ACS Nano*, 2011, **5**, 4407.
11 Z. Liu and P. C. Searson, *J. Phys. Chem. B*, 2006, **110**, 4318.
12 P. N. Ciesielski, A. M. Scott, C. J. Faulkner, B. J. Berron, D. E. Cliffel and G. K. Jennings, *ACS Nano*, 2008, **2**, 2465.
13 T.-Y. Shin, S.-H. Yoo and S. Park, *Chem. Mater.*, 2008, **20**, 5682.
14 M. M. Biener, J. Biener, A. Wichmann, A. Wittstock, T. F. Baumann, M. Bäumer and A. V. Hamza, *Nano Lett.*, 2011, **11**, 3085.
15 S. V. Petegem, S. Brandstetter, R. Maass, A. M. Hodge, B. S. El-Dasher, J. Biener, B. Schmitt, C. Borca and H. V. Swygenhoven, *Nano Lett.*, 2009, **9**, 1158.
16 Z. H. Zhang, Y. Wang, Z. Qi, J. K. Lin and X. F. Bian, *J. Phys. Chem. C*, 2009, **113**, 1308.
17 J.-F. Huang and M.-C. Fan, *J. Mater. Chem.*, 2010, **20**, 1431.
18 L. F. Liu, R. Scholz, E. Pippel and U. Gosele, *J. Mater. Chem.*, 2010, **20**, 5621.
19 H.-J. Jin, X.-L. Wang, S. Parida, K. Wang, M. Seo and J. Weissmüller, *Nano Lett.*, 2010, **10**, 187.
20 H. J. Qiu, L. Lu, L. Y. Xue and X. R. Huang, *Electrochim. Acta*, 2010, **55**, 6081.
21 H. J. Qiu, Y. L. Sun, X. R. Huang and Y. B. Qu, *Colloids Surf., B*, 2010, **79**, 304.
22 G. S. Attard, P. N. Bartlett, N. R. B. Coleman, J. M. Elliott, J. R. Owen and J. H. Wang, *Science*, 1997, **278**, 838.
23 J. H. Yuan, K. Wang and X. H. Xia, *Adv. Funct. Mater.*, 2005, **15**, 803.
24 C. Li, G. Hong and L. Qi, *Chem. Mater.*, 2010, **22**, 476.
25 Y. Ding, Y. J. Kim and J. Erlebacher, *Adv. Mater.*, 2004, **16**, 1897.
26 J. Erlebacher, M. J. Aziz, A. Karma, N. Dimitrov and K. Sieradzki, *Nature*, 2001, **410**, 450.
27 S. Van Petegem, S. Brandstetter, R. Maass, A. M. Hodge, B. S. El-Dasher, J. Biener, B. Schmitt, C. Borca and H. Van Swygenhoven, *Nano Lett.*, 2009, **9**, 1158.
28 J. Biener, A. M. Hodge, J. R. Hayes, C. A. Volkert, L. A. Zepeda-Ruiz, A. V. Hamza and F. F. Abraham, *Nano Lett.*, 2006, **6**, 2379.
29 A. Wittstock, V. Zielasek, J. Biener, C. M. Friend and M. Baumer, *Science*, 2010, **327**, 319.
30 H. J. Qiu, C. X. Xu, X. R. Huang, Y. Ding, Y. B. Qu and P. J. Gao, *J. Phys. Chem. C*, 2009, **113**, 2521.
31 H. J. Qiu, L. Y. Xue, G. L. Ji, G. P. Zhou, X. R. Huang, Y. B. Qu and P. J. Gao, *Biosens. Bioelectron.*, 2009, **24**, 3014.
32 L. H. Qian and M. W. Chen, *Appl. Phys. Lett.*, 2007, **91**, 083105.
33 Y. Ding and J. Erlebacher, *J. Am. Chem. Soc.*, 2003, **125**, 7772.
34 H. J. Qiu, Z. H. Zhang, X. R. Huang and Y. B. Qu, *ChemPhysChem*, 2011, **12**, 2118.
35 A. R. Denton and N. W. Ashcroft, *Phys. Rev. A: At., Mol., Opt. Phys.*, 1991, **43**, 3161.
36 O. V. Shulga, K. Jefferson, A. R. Khan, V. T. D'Souza, J. Liu, A. V. Demchenko and K. J. Stine, *Chem. Mater.*, 2007, **19**, 3902.
37 H. Qiu, C. Xu, X. Huang, Y. Ding, Y. Qu and P. Gao, *J. Phys. Chem. C*, 2008, **112**, 14781.
38 Y. H. Tan, J. R. Schallom, N. V. Ganesh, K. Fujikawa, A. V. Demchenko and K. J. Stine, *Nanoscale*, 2011, **3**, 3395.
39 H. J. Qiu, Y. Li, G. L. Ji, G. P. Zhou, X. R. Huang, Y. B. Qu and P. J. Gao, *Bioresour. Technol.*, 2009, **100**, 3837.
40 R. Zeis, T. Lei, K. Sieradzki, J. Snyder and J. Erlebacher, *J. Catal.*, 2008, **253**, 132.
41 H. M. Yin, C. Q. Zhou, C. X. Xu, P. P. Liu, X. H. Xu and Y. Ding, *J. Phys. Chem. C*, 2008, **112**, 9673.
42 M. Comotti, C. Della Pina, R. Matarrese and M. Rossi, *Angew. Chem., Int. Ed.*, 2004, **43**, 5812.
43 J. T. Zhang, P. P. Liu, H. Y. Ma and Y. Ding, *J. Phys. Chem. C*, 2007, **111**, 10382.
44 H. J. Chen and S. J. Dong, *Biosens. Bioelectron.*, 2007, **22**, 1811.
45 Y. Zou, L.-X. Sun and F. Xu, *Biosens. Bioelectron.*, 2007, **22**, 2669.
46 J. Wang and M. Musameh, *Anal. Chem.*, 2003, **75**, 2075.
47 M. Zhou, Y. M. Zhai and S. J. Dong, *Anal. Chem.*, 2009, **81**, 5603.
48 H. Qiu, L. Li, Q. Lang, F. Zou and X. Huang, *RSC Adv.*, 2012, **2**, 3548.
49 J. Yang, S. Y. Deng, J. P. Lei, H. X. Ju and S. Gunasekaran, *Biosens. Bioelectron.*, 2011, **29**, 159.